

Strain-mediated voltage control of skyrmion transport in nanoracetracks

Hao-Yuan Wang(王灏元), Xue-Feng Zhang(张雪枫), Tian Qiu(邱添), Huiting Li(李慧婷), Xiao-Ping Ma(马晓萍), Je-Ho Shim(沈帝虎), Xing-Ri Jin(金星日), and Hong-Guang Piao(朴红光)

Citation: Chin. Phys. B, 2026, 35 (**6**): 068502. DOI: 10.1088/1674-1056/ae3233
http://cpb.iphy.ac.cn; http://iopscience.iop.org/cpb

What follows is a list of articles you may be interested in

Spatial electron-spin splitting in single-layered semiconductor microstructure modulated by Dresselhaus spin-orbit coupling

Jia-Li Chen(陈嘉丽), Sai-Yan Chen(陈赛艳), Li Wen(温丽), Xue-Li Cao(曹雪丽), and Mao-Wang Lu(卢卯旺)

Chin. Phys. B, 2024, 33 (**11**): 118501. DOI: 10.1088/1674-1056/ad6b83

Temperature dependence of spin pumping in YIG/NiO_x/W multilayer

Lijun Ni(倪丽君), Wenqiang Wang(王文强), Lichuan Jin(金立川), Jiandong Ye(叶建东), Hehe Gong(巩贺贺), Xiang Zhan(战翔), Zhendong Chen(陈振东), Longlong Zhang(张龙龙), Xingze Dai(代兴泽), Yao Li(黎遥), Rong Zhang(张荣), Yi Yang(杨燚), Huaiwu Zhang(张怀武), Ronghua Liu(刘荣华), Lina Chen(陈丽娜), and Yongbing Xu(徐永兵)

Chin. Phys. B, 2022, 31 (**12**): 128504. DOI: 10.1088/1674-1056/ac6333

Spin transport in epitaxial Fe_3O_4/GaAs lateral structured devices

Zhaocong Huang(黄兆聪), Wenqing Liu(刘文卿), Jian Liang(梁健), Qingjie Guo(郭庆杰), Ya Zhai(翟亚), and Yongbing Xu(徐永兵)

Chin. Phys. B, 2022, 31 (**6**): 068505. DOI: 10.1088/1674-1056/ac4903

The 50 nm-thick yttrium iron garnet films with perpendicular magnetic anisotropy

Shuyao Chen(陈姝瑶), Yunfei Xie(谢云飞), Yucong Yang(杨玉聪), Dong Gao(高栋), Donghua Liu(刘冬华), Lin Qin(秦林), Wei Yan(严巍), Bi Tan(谭碧), Qiuli Chen(陈秋丽), Tao Gong(龚涛), En Li(李恩), Lei Bi(毕磊), Tao Liu(刘涛), and Longjiang Deng(邓龙江)

Chin. Phys. B, 2022, 31 (**4**): 048503. DOI: 10.1088/1674-1056/ac4cc4

Magnetoresistance effect in vertical NiFe/graphene/NiFe junctions

Pei-Sen Li(李裴森), Jun-Ping Peng(彭俊平), Yue-Guo Hu(胡悦国), Yan-Rui Guo(郭颜瑞), Wei-Cheng Qiu(邱伟成), Rui-Nan Wu(吴瑞楠), Meng-Chun Pan(潘孟春), Jia-Fei Hu(胡佳飞), Di-Xiang Chen(陈棣湘), and Qi Zhang(张琦)

Chin. Phys. B, 2022, 31 (**3**): 038502. DOI: 10.1088/1674-1056/ac192e

---

Strain-mediated voltage control of skyrmion transport in nanoracetracks

Hao-Yuan Wang(王灏元)[1,2,†], Xue-Feng Zhang(张雪枫)[1,2,†], Tian Qiu(邱添)[1,3,†], Huiting Li(李慧婷)[1,2], Xiao-Ping Ma(马晓萍)[1,2,‡], Je-Ho Shim(沈帝虎)[1,2], Xing-Ri Jin(金星日)[1,2], and Hong-Guang Piao(朴红光)[1,2,§]

[1] *Department of Physics, College of Science, Yanbian University, Yanji* 133002, *China*
[2] *Institute of Quantum Science and Technology, Yanbian University, Yanji* 133002, *China*
[3] *Hefei National Laboratory, University of Science and Technology of China, Hefei* 230088, *China*

(Received 30 September 2025; revised manuscript received 30 December 2025; accepted manuscript online 31 December 2025)

A voltage-gated scheme for controlling the transport of skyrmions in nanoracetracks is proposed using micromagnetic simulations. The scheme utilizes strain-mediated voltage control of magnetism to effectively modulate local magnetic parameters, including perpendicular magnetic anisotropy, exchange stiffness, the Dzyaloshinskii–Moriya interaction, and saturation magnetization. To understand the effect of voltage-controlled magnetism on skyrmion transport, the dynamic behavior of skyrmions was investigated by varying local magnetic parameters at different driving current densities, thereby revealing the underlying physical mechanism. The results demonstrate that skyrmion annihilation, trapping, blocking, and unblocking can be effectively controlled by coordinating the driving current with the local magnetic parameters. Our scheme offers a practical, low-power electrical control strategy for designing spintronic devices based on skyrmion dynamics.

Keywords: spintronics, skyrmions, voltage-controlled magnetism, electrostriction

PACS: 85.75.–d, 75.70.Kw, 72.25.–b, 75.85.+t

DOI: 10.1088/1674-1056/ae3233 **CSTR:** 32038.14.CPB.ae3233

Magnetic skyrmions are nontrivial magnetic textures with topological protection characteristics.[1–4] They exhibit remarkable stability and resistance to external disturbances in patterned magnetic nanostructures, and their dynamic behaviors can be driven and manipulated with relatively low current densities.[5–14] These features make them promising candidates as information carriers in next-generation spintronic devices, such as racetrack memories, logic gates, and neuromorphic computing units.[15–21] When subjected to external excitations such as spin-polarized currents, thermal gradients, or electric fields, skyrmions exhibit rich nonlinear dynamic characteristics, especially in non-uniform potential landscapes, presenting diverse and complex motion patterns.[22–27] These nonlinear dynamic responses provide novel mechanisms and strategies for designing low-power, reconfigurable spintronic devices.

In recent years, strain-mediated voltage-controlled magnetism (SVM), based on the strain-mediated magnetoelectric coupling effect, has emerged as a promising approach for the development of spintronic devices due to its numerous advantages, including low power consumption, fast response speed, and excellent material compatibility.[27–31] Generally, SVM is more readily achievable in multiferroic multilayer heterostructure systems composed of different ferroic materials, such as ferroelectric, ferromagnetic, and ferroelastic layers. As a typical example, the heterostructure composed of ferromagnetic layers and $Pb(Mg_{1/3}Nb_{2/3})_{0.7}Ti_{0.3}O_3$ (PMN-PT) can generate self-deformation through the electrostrictive effect of PMN-PT to influence the adjacent magnetic layers.[32–34] Thus, it can effectively modulate various magnetic parameters of the ferromagnetic layers, such as magnetic anisotropy (K_u), exchange stiffness (A_{ex}), Dzyaloshinskii–Moriya interaction (DMI), and saturation magnetization (M_s).[24,35–37] This SVM method enables efficient control over spin textures such as domain walls, magnetic vortices, and skyrmions.[23,38–40] Recent studies have demonstrated that the local SVM method can effectively modulate the size of skyrmions and significantly influence their dynamic characteristics, offering considerable potential for applications in logic gates, racetrack memories, and various reconfigurable nanodevices.[16,41–45] However, multi-magnetic-parameter changes caused by strain-mediated magnetoelectric coupling inevitably lead to complex couplings among magnetic parameters in a magnetic system. In skyrmion-based spintronic devices, this complex coupling behavior significantly affects the topological stability and dynamic behaviors of skyrmions, posing numerous technical challenges for their manipulation. Therefore, establishing a multi-magnetic-parameter coupling model under the SVM framework and comprehensively understanding its influence on the topological structure and dynamic behavior

[†]These authors contributed equally to this work.
[‡]Corresponding author. E-mail: xpma1222@ybu.edu.cn
[§]Corresponding author. E-mail: hgpiao@ybu.edu.cn

© 2026 Chinese Physical Society and IOP Publishing Ltd. All rights, including for text and data mining, AI training, and similar technologies, are reserved.

of skyrmions is of great theoretical significance and practical value for designing low-power, reconfigurable skyrmion spintronic devices.

To gain a deeper understanding of the influence of different magnetic parameters and their coupling effects on the dynamic behavior of skyrmions, this work systematically investigated the impact of local magnetic parameters on the topological spin structure and dynamics of spin-current-driven skyrmions in ferromagnetic nanoracetracks using the SVM method. The results revealed that the transport behavior of skyrmions can be manipulated in four ways: annihilation, trapping, blocking, and unblocking, through the regulation of local magnetic parameters. Moreover, it was found that the transport behavior of skyrmions driven by spin-polarized current can be more precisely and effectively controlled by jointly adjusting multiple magnetic parameters. This provides design strategies and parameter optimization guidelines for developing low-power, reconfigurable, and electrically controlled skyrmion devices.

Using micromagnetic simulations (MuMax3),[46] we designed a skyrmion device based on a local voltage gate and observed controllable skyrmion transport behaviors under SVM modulation in a ferromagnetic nanoracetrack. As shown in Fig. 1(a), the nanoracetrack dimensions are $400\times40\times1$ nm^3 with a mesh resolution of $2\times2\times1$ nm^3, and the SVM gate with dimensions of $60\times40\times1$ nm^3 was placed at the central region. An Ir/Co/Pt trilayer was chosen to suppress excessive spin–orbit torques (SOT) while retaining a finite interfacial DMI due to the asymmetric sputtered interfaces. In the simulations, only the magnetic properties of the 1 nm Co layer were considered.[46–49] For simplicity, effective Co material parameters were used to represent the multilayer system.[50] Specifically, the material constants were set as follows: saturation magnetization $M_s = 580$ kA/m, exchange stiffness coefficient $A_{ex} = 15$ pJ/m, Gilbert damping constant $\alpha = 0.3$, and interface DMI constant $D = 3.5$ mJ/m^2. The uniaxial perpendicular magnetic anisotropy (PMA) constant is $K_u = 0.8\times10^6$ J/m^3. The local magnetic parameters at the SVM gate are modulated by the applied voltage (V_{gate}) through the strain-mediated magnetoelectric coupling effect. We assume that under the gate voltage, the adjustable range of the local magnetic parameters in the SVM gate region is $K_u^v = (0.4\sim1.2)K_u$, $A_{ex}^v = (0.5\sim1.5)A_{ex}$, $M_s^v = (0.5\sim1.5)M_s$, and $D^v = (0.5\sim1.5)D$. Initially, a Néel-type skyrmion was introduced at the left end of the nanoracetrack. The transport behavior of skyrmions is driven by the spin transfer torque (STT) effect along the $+x$ axis, as indicated by the yellow arrow in Fig. 1(a).[51–54] The current density J_c was varied from $4\times10^{11}\sim12\times10^{11}$ A/m^2 with $\beta = 0.3$.

Firstly, the influence of modulating only the local PMA (K_u^v) in the SVM gate region on skyrmion transport under various driving current densities (J_c) was examined. As shown in Fig. 1(b), applying a positive voltage such that $K_u^v > K_u$ results in the formation of a potential barrier in the gate region (red curve), which can effectively block skyrmions from entering. Conversely, when a negative voltage is applied, making $K_u^v < K_u$, a potential well forms (blue curve). This allows skyrmions to enter the SVM gate region but can hinder their escape, thereby facilitating their trapping within the gate (yellow area).

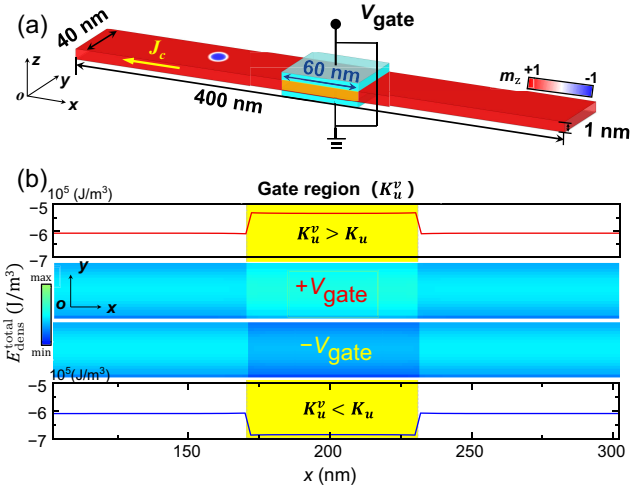


Fig. 1. (a) Schematic of the voltage-gated skyrmion nanotrack. The blue region indicates the gate-controlled area, where the PMA (K_u^v) is tuned by the applied voltage. A spin-polarized current $\boldsymbol{J}_c$, represented by the yellow arrow, is injected along the $-x$ direction to drive the skyrmion motion. The color scale (red to blue) denotes the out-of-plane magnetization component ($\boldsymbol{m}_z$). (b) Total energy density (E_{dens}^{total}) profiles in the gate region under different voltage polarities. A positive gate voltage ($+V_{gate}$) increases the anisotropy ($K_u^v > K_u$), while a negative gate voltage ($-V_{gate}$) reduces it ($K_u^v < K_u$). The corresponding redistribution of local anisotropy and energy density is illustrated.

We systematically investigated the effect of varying the local PMA K_u^v within the range of $0.8K_u$ to $1.2K_u$ under different driving current densities J_c. Interestingly, it was observed that modulation of K_u^v in the SVM gate region enables distinct modes of control over skyrmion motion, as shown in Fig. 2(a). These include annihilation (Case 1), trapping (Case 2), unblocking (Case 3), and blocking (Case 4), as illustrated in Figs. 2(b)–2(e). For example, under a driving current density of $J_c = 7\times10^{11}$ A/m^2, skyrmions are annihilated within the SVM gate region when $K_u^v/K_u \le 0.86$; trapped when $0.86 < K_u^v/K_u \le 0.94$; unblocked when $0.94 < K_u^v/K_u \le 1.05$; and blocked when $K_u^v/K_u > 1.05$.

The voltage-induced reconstruction of the local anisotropy energy landscape within the gate region provides a consistent explanation for these phenomena. When $K_u^v/K_u \le 0.86$, the perpendicular magnetic anisotropy inside the gate is significantly reduced compared with that of the nanotrack, leading to a substantial decrease in anisotropy energy and the formation of a deep local energy minimum. Under these conditions, skyrmions become energetically unfavorable once they enter the gate region. Their spin configurations become unstable, and the topologically protected

structures collapse into locally distorted multidomain states, leading to the annihilation regime. In the intermediate range $0.86 < K_u^v/K_u \leq 0.94$, although the anisotropy reduction is insufficient to destroy the skyrmion topology, it still produces a finite potential well. Consequently, once a skyrmion enters the gated region, it becomes energetically confined and stabilizes near the gate center, corresponding to the trapping regime. When $0.94 < K_u^v/K_u \leq 1.05$, the anisotropy contrast between the gate and the surrounding track further decreases, and the potential well evolves into a shallow barrier. The trapping effect disappears, allowing the skyrmion to traverse the gate under current drive and exhibit continuous transport, corresponding to the unblocking regime. For $K_u^v/K_u > 1.05$, the anisotropy inside the gate exceeds that of the track and forms a pronounced energy barrier. As the skyrmion approaches the left boundary of the gate, its forward motion is strongly inhibited, and it eventually becomes immobilized at the boundary if the driving torque is insufficient to overcome the barrier, leading to the blocking regime.

More notably, as J_c increases, the regulatory ranges for annihilation (Case 1) and unblocking (Case 3) gradually expand, whereas those for trapping (Case 2) and blocking (Case 4) shrink. In particular, the trapping region (Case 2) nearly vanishes at $J_c = 12 \times 10^{11}$ A/m^2. This trend suggests that, under the competition between current-driven energy and the energy associated with the potential barrier or well, annihilation and unblocking become the dominant skyrmion transport behaviors at higher current densities within the limited SVM control framework.

To further elucidate the underlying dynamics of skyrmion transport, the trajectories of skyrmions, their diameter evolution, and their energy responses to SVM gate modulation were analyzed. Figures 3(a) and 3(b) present two representative cases corresponding to the application and removal of the gate voltage. When $K_u^v/K_u = 0.9$, the locally reduced anisotropy within the gate drives the skyrmion into the gated region, where it relaxes into a metastable confined state. In this case, both the skyrmion diameter and trajectory exhibit pronounced oscillations. By contrast, when $K_u^v/K_u = 1.1$, the enhanced anisotropy acts as a robust potential barrier, preventing the skyrmion from penetrating the gate. Consequently, the skyrmion remains pinned near the left boundary, showing only minor changes in position and diameter. This highly stable configuration highlights its potential for non-volatile information storage.

Figures 3(c) and 3(d) compare the competition between anisotropy energy (E_{anis}) and interfacial energy ($E_{\text{inter}} = E_{\text{exch}} + E_{\text{demag}}$). The results reveal that trapping and blocking originate from distinct energy balances. In the trapping regime, the oscillatory fluctuations arise from dynamic compensation between increased E_{anis} and reduced E_{inter} induced by local anisotropy modulation. By contrast, in the blocking regime, the anisotropy barrier dominates the interfacial contribution, resulting in nearly stable energy profiles and preventing skyrmion penetration. Trapping enables easier detection but increases the risk of annihilation under high current densities, whereas blocking ensures robust stability at the expense of reduced observability. Thus, tailoring the balance between anisotropy and interfacial energies provides an effective route toward voltage-controlled skyrmion manipulation.

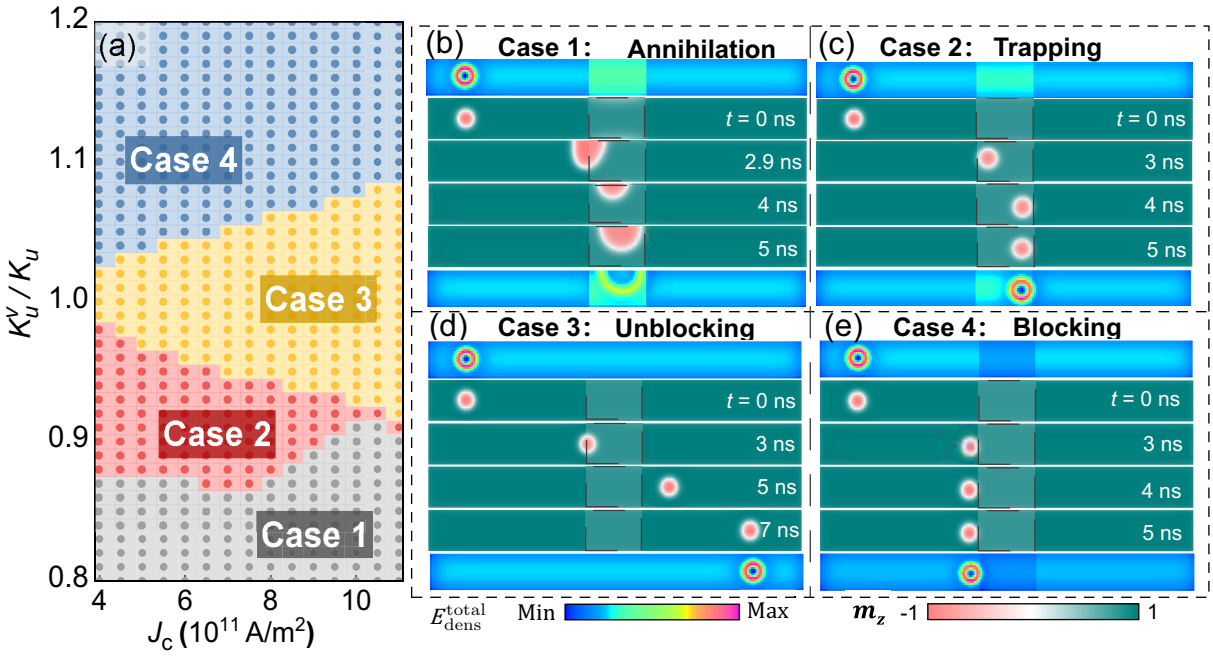


Fig. 2. (a) Phase diagram of skyrmion dynamical behaviors as a function of the driving current density J_c and the anisotropy ratio in the gate region K_u^v/K_u, indicating four typical skyrmion dynamic behavior regimes. (b)–(e) Representative snapshots of skyrmion evolution in each regime: (b) Case 1: Annihilation, (c) Case 2: Trapping, (d) Case 3: Unblocking, and (e) Case 4: Blocking.

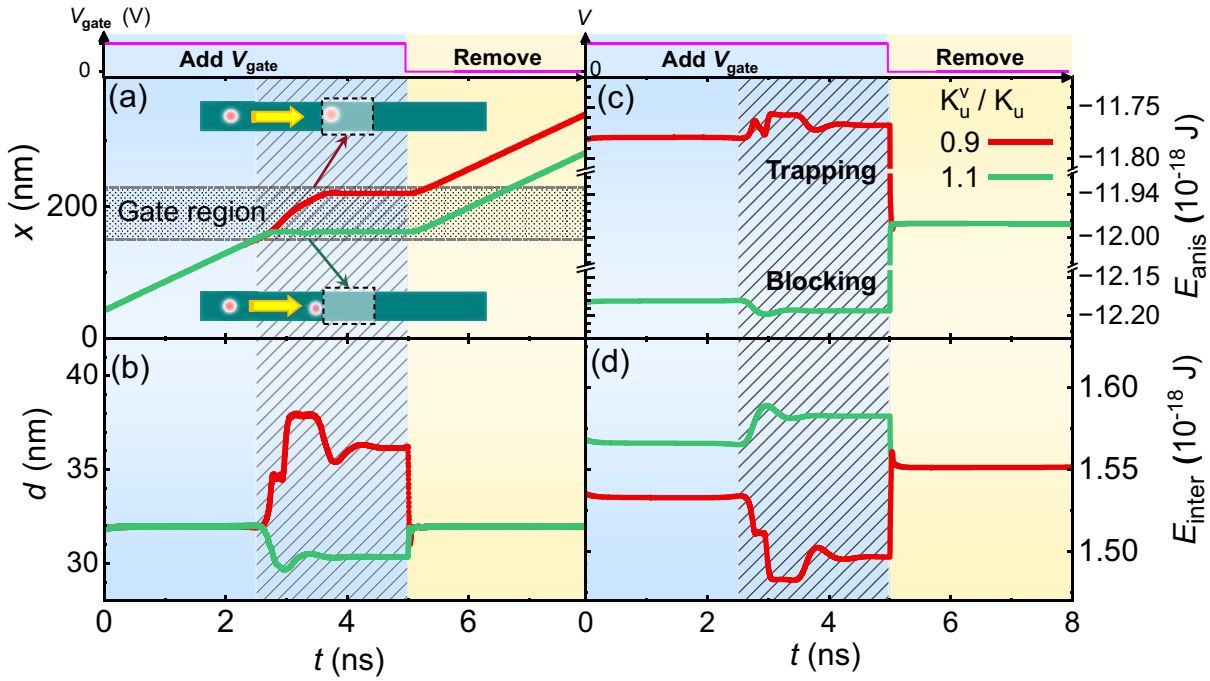


Fig. 3. Skyrmion dynamics and energy evolution under gate voltage modulation for low ($K_u^v/K_u = 0.9$, red) and high ($K_u^v/K_u = 1.1$, green) anisotropy. Blue and yellow regions indicate gate voltage on (t = 0–5 ns) and off (t = 5–8 ns), respectively. The hatched region corresponds to the dynamical processes of the skyrmion within the gate region. (a) Skyrmion position along the x direction; the grey region indicates the corresponding gate position. (b) Time evolution of the skyrmion diameter. (c) Anisotropy energy E_{anis} with spatial distributions for trapping (top) and blocking (bottom). (d) Total interfacial energy $E_{inter} = E_{exch} + E_{demag}$.

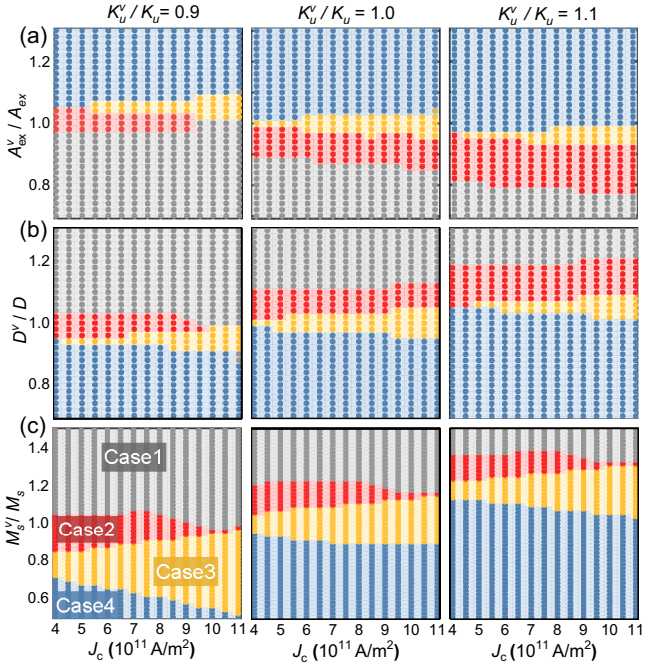


Fig. 4. Phase diagrams showing the influence of local magnetic parameters on skyrmion transport behavior for anisotropy ratios $K_u^v/K_u = 0.9$, 1.0, and 1.1 in the gate region. (a) Relative exchange stiffness ratio A_{ex}^v/A_{ex}, (b) DMI strength ratio D^v/D, and (c) saturation magnetization ratio M_s^v/M_s. The different colors correspond to four typical skyrmion behaviors: Case 1 (gray area, annihilation), Case 2 (red area, trapping), Case 3 (yellow area, unblocking), and Case 4 (blue area, blocking).

As is well known, voltage application modulates not only the PMA K_u^v in the gate region, but also alters the local energy distribution and structural stability of the system. Moreover, voltage induces synchronous modulations in the local exchange stiffness A_{ex}, DMI strength D, and saturation magnetization M_s, mediated by mechanisms such as interfacial charge reconstruction, ion migration, or strain effects. To elucidate the coupling between these magnetic parameters and PMA, three representative PMA ratios (K_u^v/K_u = 0.9, 1.0, and 1.1) were selected. Under a current density of J_c = 4–11 $\times$ 10^{11} A/m^2, the system was scanned over a parameter space including A_{ex}^v/A_{ex}, D^v/D, and M_s^v/M_s to map the corresponding skyrmion dynamical behaviors (Case 1–4). For a more precise comparison of the influence of these variables on skyrmion modulation, K_u^v was jointly varied with A_{ex}^v, D^v, and M_s^v to analyze skyrmion dynamics under two-parameter variations.

Figure 4(a) presents the skyrmion phase diagram on the A_{ex}^v/A_{ex}–J_c plane under three gate PMA conditions (K_u^v/K_u = 0.9, 1.0, and 1.1). As both A_{ex}^v/A_{ex} and K_u^v/K_u increase, the annihilation region (Case 1) shrinks, while the trapping (Case 2) and blocking (Case 4) regions expand. Increasing the ratio A_{ex}^v/A_{ex} drives the total energy density in the gate region toward more negative values. The potential well inside the gate becomes shallower (the potential barrier becomes deeper) compared to the unmodulated case, as shown in Fig. 5(a). This strengthens the topological stability of skyrmions once they enter the gate, diminishes the annihilation region, and expands the trapping areas. As a result, skyrmions are more readily halted at the gate boundary (Case 4). In parallel, the cooperative effect of strengthened PMA and reduced exchange stabilizes the skyrmion within the gate, thereby enlarging the trap-

ping regime (Case 2) and promoting robust confinement.

Figure 4(b) shows the skyrmion phase diagram on the D^v/D–J_c plane under three levels of PMA conditions ($K_u^v/K_u = 0.9$, 1.0, and 1.1). In contrast to the exchange modulation in Fig. 4(a), an opposite trend is observed: as D^v/D decreases and K_u^v/K_u increases, the skyrmion behavior evolves from annihilation (Case 1) to blocking (Case 4), with a concurrent expansion of the trapping region (Case 2). This highlights the distinct role of interfacial DMI in governing chiral exchange interactions. Specifically, tuning D^v/D modifies the energy density profile at the gate–track interface. As shown in Fig. 5(b), a characteristic redistribution of the potential landscape occurs. For example, when D^v/D increases, the outer energy peak rises while the inner peak decreases, corresponding respectively to barrier suppression and barrier enhancement, as the skyrmion enters the gate. The energetic cost of maintaining the spin rotation increases, making skyrmions more prone to morphological distortion and even topological annihilation. Under these conditions, the annihilation region in the phase diagram is significantly enlarged. Conversely, moderate or reduced D^v/D suppresses internal chirality and stabilizes the skyrmion structure. At the same time, pronounced spin distortions and a localized increase in exchange concentration near the gate boundary elevate the outer potential barrier, thereby enhancing the blocking effect and preventing skyrmion penetration.

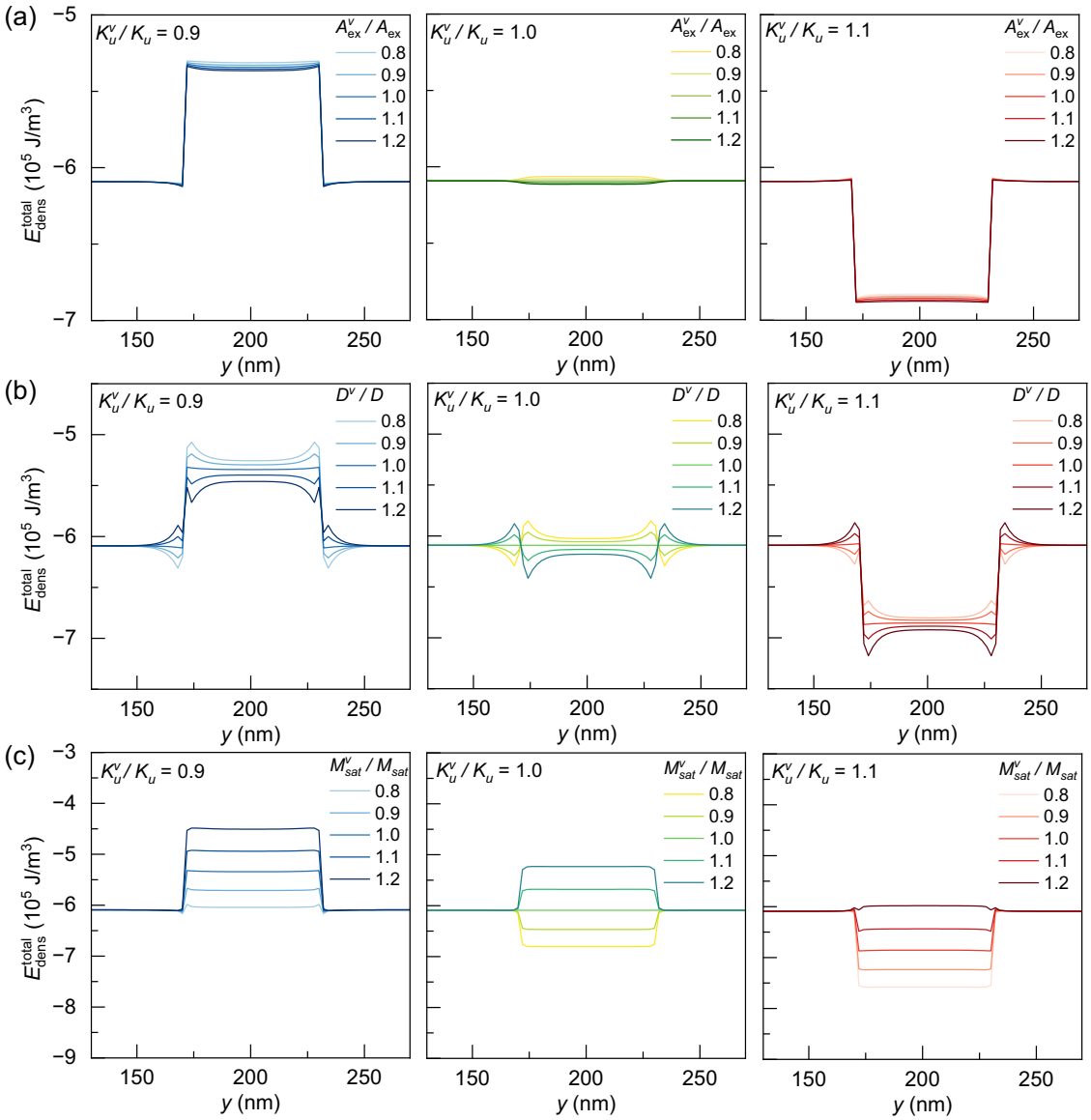


Fig. 5. Evolution of the total energy density distribution in the gate region under different PMA ratios $K_u^v/K_u = 0.9$, 1.0, and 1.1. (a) Relative exchange stiffness ratio A_{ex}^v/A_{ex}, (b) DMI strength ratio D^v/D, and (c) saturation magnetization ratio M_s^v/M_s.

Figure 4(c) presents the skyrmion dynamical phase diagram in the M_s^v/M_s–J_c plane under three PMA conditions ($K_u^v/K_u = 0.9$, 1.0, and 1.1). A clear transition occurs with increasing M_s^v/M_s, where the dominant behavior shifts from blocking (Case 4) to annihilation (Case 1). This evolution highlights the critical influence of M_s^v-induced modifications on the local energy landscape. As shown in Fig. 5(c), increasing the ratio M_s^v/M_s raises the total energy density in the gate

region and effectively deepens the potential well while reducing the barrier height. Under these conditions, skyrmion motion is strongly modulated: the deeper potential well lowers the energetic barrier, making skyrmions more susceptible to topological instability and enlarging the annihilation region. Conversely, reducing M_s^v/M_s effectively increases the energy barrier within the gate, which suppresses local spin texture distortions and favors the preservation of skyrmion topology, while simultaneously reinforcing blocking at the gate boundary (Case 4). Furthermore, at a fixed M_s^v/M_s, stronger PMA ($K_u^v/K_u > 1$) increases the effective energy barrier, suppresses the trapping regime (Case 2), and enlarges the blocking region (Case 4). This indicates that PMA reinforcement counteracts the destabilizing influence of M_s^v, thereby maintaining higher energy barriers that constrain skyrmion deformation and prevent collapse.

We find that the synergistic variation of multiple magnetic parameters not only significantly modifies the phase boundaries of the four skyrmion behavior modes (Cases 1–4), but also reveals the intricate energy competition between potential-well formation and topological protection. These results highlight the importance of considering multi-physical coupling effects induced by voltage regulation in practical device design and optimization, particularly the non-local responses arising from strain reconstruction and the electric-field-induced covariation of magnetic parameters. These findings provide theoretical support for achieving stable, low-energy skyrmion memory and logic devices and further suggest that, when selecting materials for skyrmion applications, attention should be paid to the collective regulation of magnetic properties in heterogeneous material systems.

In summary, this work systematically investigates the SVM modulation of skyrmion transport in nanoracetracks by locally tuning key magnetic parameters, including anisotropy, exchange stiffness, DMI, and saturation magnetization. Four distinct transport behaviors were identified: annihilation, trapping, unblocking, and blocking. Dual-parameter phase diagrams demonstrate that each regime originates from a subtle balance between PMA and interfacial energy contributions (exchange, DMI, and demagnetization). Under voltage gating, the coupling among magnetic parameters induces energy gradients and spin-texture deformations, which critically determine the stability and dynamics of skyrmions. These findings underscore the importance of considering voltage-controlled magnetism interactions and parameter covariation in device design, providing theoretical support for low-power, reconfigurable, and electrically tunable skyrmion-based memory and logic applications in next-generation spintronic devices.

Acknowledgments

Project supported by the National Natural Science Foundation of China (Grant No. 12364020), the Scientific and Technological Development Plan of Jilin Province (Grant No. 20240101295JC), and the Applied Foundation Research Project (Talent Funding Project) of Yanbian University (Grant No. ydkj202241).

References

[1] Tokura Y and Kanazawa N 2020 *Chem. Rev.* **121** 2857
[2] Bogdanov A N and Panagopoulos C 2020 *Nat. Rev. Phys.* **2** 492
[3] Wang K, Huang Y, Zhang X, Zhou Y and Zhao W 2016 *Proc. IEEE* **104** 2040
[4] Nagaosa N and Tokura Y 2013 *Nat. Nanotechnol.* **8** 899
[5] Wang X S, Yuan H Y and Wang X R 2018 *Commun. Phys.* **1** 31
[6] Göbel B, Mertig I and Tretiakov O A 2021 *Phys. Rep.* **895** 1
[7] Tan A K C, Weigand M, Büttner F, Günther C M, Gräfe J, Eisebitt S and Beach G S D 2021 *Nat. Commun.* **12** 4252
[8] Sampaio J, Cros V, Rohart S, Fert A and Thiaville A 2013 *Nat. Nanotechnol.* **8** 839
[9] Komineas S and Papanicolaou N 2015 *Phys. Rev. B* **92** 064412
[10] Hrabec A, Sampaio J, Belmeguenai M, Gross I, Weil R, Cherif S M, Stashkevich A, Jacques V, Thiaville A and Rohart S 2017 *Nat. Commun.* **8** 15765
[11] Juge R, Je S G, de Souza Chaves D, *et al.* 2019 *Phys. Rev. Appl.* **12** 044007
[12] Woo S, Song K M, Zhang X, Zhou Y, Ezawa M, Liu X, Finizio S, Raabe J, Lee N J, *et al.* 2018 *Nat. Commun.* **9** 959
[13] Tang J, Wu Y, Wang W, Kong L, Lv B, Wei W, Zang J, Tian M and Du H 2021 *Nat. Nanotechnol.* **16** 1086
[14] Ye C, Li L L, Shu Y, Li Q R, Xia J, Hou Z P, Zhou Y, Liu X X, Yang Y Y and Zhao G P 2022 *Rare Met.* **41** 2200
[15] Tomasello R, Martinez E, Zivieri R, Torres L, Carpentieri M and Finocchio G 2014 *Sci. Rep.* **4** 6784
[16] Wang K, Zheng C, Huang Y, Zhang X, Zhou Y and Lv W 2016 *IEEE Electron Device Lett.* **37** 924
[17] Song K M, Jeong J S, Pan B, Zhang X, Xia J, Cha S, Park J E, Kim K, Finizio S, *et al.* 2020 *Nat. Electron.* **3** 148
[18] Luo S, Song M, Li X, Zhang Y, Hong J, Yang X, Zou X, Xu N and You L 2018 *Nano Lett.* **18** 1180
[19] Zhang X, Ezawa M and Zhou Y 2015 *Sci. Rep.* **5** 9400
[20] Fert A, Reyren N and Cros V 2017 *Nat. Rev. Mater.* **2** 17031
[21] Finocchio G, Büttner F, Tomasello R, Carpentieri M and Kläui M 2016 *J. Phys. D: Appl. Phys.* **49** 423001
[22] Zhang S L, Wang W, Burn D M, Peng H, Berger H, Bauer A, Pfleiderer C, van der Laan G and Hesjedal T 2018 *Nat. Commun.* **9** 2115
[23] Xia H, Song C, Jin C, Wang J, Wang J and Liu Q 2018 *J. Magn. Magn. Mater.* **458** 57
[24] Gorshkov I O, Gorev R V, Sapozhnikov M V and Udalov O G 2022 *ACS Appl. Electron. Mater.* **4** 3205
[25] Wang K, Bheemarasetty V, Duan J, Zhou S and Xiao G 2022 *J. Magn. Magn. Mater.* **563** 169905
[26] Ma X P, Li H T, Zhang X F, Li C F, Shim J H and Piao H G 2025 *Appl. Phys. Lett.* **126** 142401
[27] Mishra P K, Sravani M, Bose A and Bhuktare S 2024 *J. Appl. Phys.* **135** 220701
[28] Nozaki T, Yamamoto T, Miwa S, Tsujikawa M, Shirai M, Yuasa S and Suzuki Y 2019 *Micromachines* **10** 327
[29] Rana B and Otani Y 2019 *Commun. Phys.* **2** 90
[30] Amiri P K and Wang K L 2012 *Spin* **2** 1240002
[31] Bhattacharya D, Bandyopadhyay S and Atulasimha J 2019 *Multifunct. Mater.* **2** 032001
[32] Zhang Y, Sun W, Cao K, *et al.* 2024 *Sci. Adv.* **10** eadl4633
[33] Chen A, Piao H G, Zhang C, Ma X P, Algaidi H, Ma Y, Li Y, Zheng D, Qiu Z and Zhang X X 2023 *Mater. Horiz.* **10** 3034
[34] Chen A, Piao H G, Ji M, Fang B, Wen Y, Ma Y, Li P and Zhang X X 2021 *Adv. Mater.* **33** 2105902
[35] Cho J, Miwa S, Yakushiji K, Kubota H, Fukushima A, You C Y, Yuasa S and Suzuki Y 2018 *Phys. Rev. Appl.* **10** 014033
[36] Schott M, Ranno L, Béa H, Baraduc C, Auffret S and Bernand-Mantel A 2021 *J. Magn. Magn. Mater.* **520** 167122
[37] Srivastava T, Schott M, Juge R, *et al.* 2018 *Nano Lett.* **18** 4871
[38] Ba Y, Zhuang S, Zhang Y, *et al.* 2021 *Nat. Commun.* **12** 322

[39] Franke K J A, Van de Wiele B, Shirahata Y, Hämäläinen S J, Taniyama T and van Dijken S 2015 *Phys. Rev. X* **5** 011010
[40] Xing X, Pong P W T and Zhou Y 2016 *Phys. Rev. B* **94** 054408
[41] Tan F N, Gan W L, Ang C C I, Wong G D H, Liu H X, Poh F and Lew W S 2019 *Sci. Rep.* **9** 7369
[42] Parkin S S P, Hayashi M and Thomas L 2008 *Science* **320** 190
[43] Zhang X, Zhou Y, Ezawa M, Zhao G P and Zhao W 2015 *Sci. Rep.* **5** 11369
[44] Paul S and Heinze S 2022 *npj Comput. Mater.* **8** 105
[45] Wang K, Huang Y, Zheng C, Lv W, Lei N, Zhang Y, Zhang X, Zhou Y and Zhao W 2016 *Sci. Rep.* **6** 23164
[46] Vansteenkiste A, Leliaert J, Dvornik M, Helsen M, Garcia-Sanchez F and Van Waeyenberge B 2014 *AIP Adv.* **4** 107133
[47] Moreau-Luchaire C, Moutafis C, Reyren N, Sampaio J, Vaz C A F, Van Horne N, Bouzehouane K, Garcia K, Deranlot C, *et al.* 2016 *Nat. Nanotechnol.* **11** 444
[48] Pham V T, Sisodia N, Di Manici I, Urrestarazu-Larrañaga J, Bairagi K, Pelloux-Prayer J, Guedas R, Buda-Prejbeanu L D, Auffret S, Locatelli A, *et al.* 2024 *Science* **384** 307
[49] Luo J, Xia J, Liang X, Zhou Y, Li L L, Gu L and Zhao G 2024 *Phys. Rev. B* **110** 214409
[50] Schott M, Bernand-Mantel A, Ranno L, Pizzini S, Vogel J, Béa H, Baraduc C, Auffret S, Gaudin G and Givord D 2017 *Nano Lett.* **17** 3006
[51] Fert A, Ramesh R, Garcia V, Casanova F and Bibes M 2024 *Rev. Mod. Phys.* **96** 015005
[52] Iwasaki J, Mochizuki M and Nagaosa N 2013 *Nat. Commun.* **4** 1463
[53] Iwasaki J, Mochizuki M and Nagaosa N 2013 *Nat. Nanotechnol.* **8** 742
[54] Ai X L, Li H T, Zhang X F, Li C F, Shim J H, Ma X P and Piao H G 2024 *Chin. Phys. B* **33** 107502